

# Modeling, equilibrium and kinetics of CO<sub>2</sub> adsorption in LTA zeolite obtained from clay

V. H. S. Ramos<sup>1</sup>, D. R. L. Vedoy<sup>2</sup>, P. C. C. de Araújo<sup>3</sup>, J. J. Marques<sup>4</sup>, P. H. L. Quintela<sup>1</sup>, E. Jesus<sup>1\*</sup>

<sup>1</sup>Federal University of Sergipe, Department of Chemical Engineering, São Cristóvão, SE, Brazil

<sup>2</sup>University of Alberta, Department of Chemical and Materials Engineering, Edmonton, Alberta, Canada

<sup>3</sup>State University of Maringá, Department of Chemical Engineering, Maringá, PR, Brazil

<sup>4</sup>Federal University of Sergipe, Department of Environmental Engineering, São Cristóvão, SE, Brazil

## Abstract

This paper discussed the synthesis of LTA zeolite from Pinheiro clay (PIN) aiming for adsorption of CO<sub>2</sub>. To obtain the LTA-PIN zeolite, the PIN was submitted to acid treatment, followed by calcination and hydrothermal treatment. These treatments promoted the reorganization of the crystalline structure of the PIN, leading to the LTA-PIN zeolite with 95.79% purity confirmed by XRD, SEM, XRF, and FTIR results. The performance of the LTA-PIN zeolite was similar to the one of the standard LTA zeolite. The CO<sub>2</sub> adsorption by the zeolites could be properly described by the pseudo-second-order kinetic and Freundlich isotherm models, suggesting that physisorption was the main mechanism responsible for the deposition of CO<sub>2</sub> at the surface of the zeolites. According to regeneration results, LTA-PIN zeolite can be reused five times without significant loss of CO<sub>2</sub> adsorption capacity, contrary to the 12% reduction in CO<sub>2</sub> adsorption capacity presented by the LTA-standard zeolite.

**Keywords:** LTA zeolite, Pinheiro clay, modeling, adsorption of CO<sub>2</sub>.

## INTRODUCTION

The latest report by the Intergovernmental Panel on Climate Change [1] showed that if there are no additional efforts to reduce emissions of greenhouse gases, especially CO<sub>2</sub>, the predicted global temperature increase of 3.7 °C could rise to 4.8 °C by 2100. In addition to the environmental issue, CO<sub>2</sub> is often considered an impurity in gas streams, which is the case in natural gas and biogas streams [2], thus there is a need to find ways to prevent its emission.

Zeolites, microporous solids of the aluminosilicate type with a crystalline structure, have been receiving attention from researchers because of their low cost, simple production, a high percentage of micropores, and their high adsorptive capacity at low pressures [3]. For these reasons, zeolites have been widely used for the capture of pollutant gases in different processes. For example, type A (LTA) [2] and type X zeolites [4] stand out among the zeolites used in the capture of CO<sub>2</sub> via adsorption. The adsorption of CO<sub>2</sub> on LTA zeolites occurs inside the pores with 4.1 Å aperture diameter by chemical or physical interaction [2, 5]. According to the International Zeolite Association (IZA), zeolites can be obtained naturally or synthetically [5]. Most synthetic zeolites are produced by the hydrothermal method using silica, alumina, and alkaline earth metals in the reaction mixture as charge compensators. Although synthetic zeolites can be obtained with high purity and crystallinity, the analytical reagents required to produce zeolites are generally expensive. Thus, several alternative

sources of silica and alumina are being tested in zeolite production to reduce synthesis costs and make the product more environmentally friendly, including natural clays [6], bentonite [7], kaolin [8], and fly ash [4]. An important step for application is to reduce the amount of components that can interfere with zeolite crystallization.

In this context, this work evaluated the use of Pinheiro clay from the State of Sergipe, Brazil, as a starting material to produce LTA zeolite for CO<sub>2</sub> adsorption applications. Few studies have investigated the use of Pinheiro clay, which offers many advantages for the synthesis of LTA zeolite, including high availability, low cost, and appropriate chemical composition (i.e., having high silica and alumina contents, which are structural components of zeolites). In addition, this work presented a model along with thermodynamic equations, which help to understand the CO<sub>2</sub> adsorption in LTA zeolite under low pressures.

## MATERIALS AND METHODS

*Clay preparation and acid treatment:* Pinheiro clay (PIN) was collected in the municipality of Laranjeiras-SE, Brazil, and ground to smaller particle size using a ball mill (SL34/3P, Solab). Next, the material recovered from a 100 mesh screen was oven-dried (Imcamo 4) at 60 °C for 12 h. An acid treatment was performed to remove exchangeable cations and organic matter present in the clay, in which 100 g of clay sample was dispersed in 500 mL of 3 mol/L HCl (Impex) and kept under agitation for 10 h at 80 °C [9]. Next, the material was vacuum filtered, washed with distilled water, dried in an oven at 80 °C for 12 h, and crushed with a mortar and pestle. The acid-treated clay (PIN-MOD) was subsequently passed

\*edilsonjs@ufs.br

 <https://orcid.org/0000-0003-4239-6050>

through a 100 mesh sieve [10] to maintain uniform particle size.

**Obtaining the LTA zeolite:** the LTA-PIN zeolite was obtained by a two-stage route of calcination and hydrothermal treatment [6]. First, 31.20 g of PIN-MOD clay (source of SiO<sub>2</sub> and Al<sub>2</sub>O<sub>3</sub>), 25.81 g of NaAlO<sub>2</sub> (Dynamic, 99.81%), and 37.43 g of NaOH (Alphatec, 99%) were mixed and then macerated until a homogeneous mixture, which was then calcined in a muffle furnace at 600 °C for different times (2, 4, or 6 h). The mixture was macerated, dissolved in 444.2 mL of distilled water forming a reaction mixture of 3.165 Na<sub>2</sub>O:Al<sub>2</sub>O<sub>3</sub>:1.926 SiO<sub>2</sub>:128.0 H<sub>2</sub>O molar composition. The mixture was aged under stirring for 1 h, transferred to a polypropylene flask, and heated to 100 °C in an oven (Imcamo 4) for different hydrothermal treatment times (2, 4, or 6 h). Finally, the mixture was cooled in an ice bath and separated by vacuum filtration. The material obtained (LTA-PIN) was washed with distilled water until pH 8-9, dried in an oven at 80 °C for 12 h, and crushed with a mortar and pestle. The LTA-standard zeolite was obtained by the conventional route [5].

**Characterizations:** the chemical composition was determined by energy dispersive X-ray fluorescence (XRF) spectroscopy (EDX-720/800HS, Shimadzu). The organic matter content was determined by the ignition method [11] and used to recalculate the chemical composition of the reaction mixture. Structural analysis was performed using X-ray diffractometry (LabX XRD-6000, Shimadzu) with CuKα radiation (λ=0.1542 nm), 30 kV voltage, 30 mA current, and 2θ angle ranging from 4° to 60°. The identification and refinement of the diffractograms were conducted using software (X'Pert HighScore, PANalytical) in comparison with the files available in the ICSD database using the Rietveld method. The crystallinity percentage of the LTA zeolite was calculated by comparing the sum of peak intensities for the d<sub>442</sub> planes at 21.67°, d<sub>622</sub> at 23.99°, d<sub>642</sub> at 27.11°, d<sub>820</sub> at 29.94°, and d<sub>664</sub> at 34.18° [12]. The cation exchange capacity was performed using the methylene blue stain method [13]. The main functional groups were analyzed via Fourier transform infrared spectroscopy (FTIR, 640-IR, Varian) using KBr pellets in the region between 4000 and 400 cm<sup>-1</sup> with a resolution of 4 cm<sup>-1</sup>. Morphological analysis was performed by scanning electron microscopy (SEM, Carry Scope JCM-5700, Jeol). The textural analysis was performed by N<sub>2</sub> physisorption (Nova 4000e, Quantachrome) with previous degassing of the sample at 150 °C for 2 h under vacuum. The actual specific mass of the adsorbents was determined by helium gas pycnometry (AccuPyc II 1340, Micromeritics) to determine the volume of the adsorbent in the adsorption system.

**CO<sub>2</sub> adsorption tests:** the tests used the static volumetric method [14, 15]. The method consisted of pressurizing a fixed-bed column (Fig. 1) containing a certain mass of adsorbent with CO<sub>2</sub> at different initial pressures. The initial pressure dropped as a consequence of the adsorption of CO<sub>2</sub> at the adsorbent surface until equilibrium was reached. This method determined the amount of CO<sub>2</sub> adsorbed by indirect measurement of the initial pressure of the system

since the volume of the column and the volume occupied by the adsorbent are known [14]. To do so, it was necessary to determine the volume occupied by free CO<sub>2</sub> inside the column, according to:

$$V_d = V_t - V_s \quad (\text{A})$$

in which V<sub>d</sub> is the volume occupied by CO<sub>2</sub> in the column (cm<sup>3</sup>), V<sub>t</sub> is the total volume of the system (138.54 cm<sup>3</sup>), and V<sub>s</sub> is the volume occupied by the adsorbent (cm<sup>3</sup>). The volume occupied by the adsorbent was determined by:

$$V_s = \frac{m_{\text{ads}}}{\tilde{n}_{\text{ads}}} \quad (\text{B})$$

in which m<sub>ads</sub> is the mass of adsorbent (g), and ρ<sub>ads</sub> is the real density of the adsorbent (g/cm<sup>3</sup>). Next, Eqs. C and D were used for calculating the number of moles at the beginning of the process and in equilibrium:

$$n_{\text{initial}} = \frac{V_d}{(V_m)_{\text{initial}}} \quad (\text{C})$$

$$n_{\text{eq}} = \frac{V_d}{(V_m)_{\text{eq}}} \quad (\text{D})$$

in which n<sub>initial</sub> is the number of moles of CO<sub>2</sub> at the beginning of the process, n<sub>eq</sub> is the number of moles of CO<sub>2</sub> in the equilibrium, V<sub>d</sub> is the volume occupied by CO<sub>2</sub> in the column (cm<sup>3</sup>), (V<sub>m</sub>)<sub>initial</sub> is the specific volume of CO<sub>2</sub> at the beginning of the process (cm<sup>3</sup>), and (V<sub>m</sub>)<sub>eq</sub> is the specific volume of CO<sub>2</sub> in the equilibrium (cm<sup>3</sup>). The state equation of the truncated virial in the second term (Eq. E) and the Pitzer correlations for the calculation of the second virial coefficient (Eqs. F to H) were used due to the low pressures employed (0.1 to 0.5 MPa) to determine the specific volume of CO<sub>2</sub> (Eq. I) both at the beginning of the process and at equilibrium:

$$Z=1+\frac{BP}{RT} \quad (\text{E})$$

$$B^0=0.083-\frac{0.422}{T_r^{1.6}} \quad (\text{F})$$

$$B^1=0.139-\frac{0.172}{T_r^{4.2}} \quad (\text{G})$$

$$B = \frac{RT_c}{P_c} (B^0 + \omega B^1) \quad (\text{H})$$

$$V_m = \frac{ZRT}{P} \quad (\text{I})$$

in which  $T_r$  is the reduced temperature,  $T_c$  is the critical temperature,  $R$  is the universal gas constant,  $P_c$  is the critical pressure,  $P$  is the initial or equilibrium pressure,  $\omega$  is the acentric factor for  $\text{CO}_2$ ,  $Z$  is the compressibility factor, and  $V_m$  is the specific volume of  $\text{CO}_2$  initially or at equilibrium. In turn, the variation in the number of moles of  $\text{CO}_2$  provided through Eqs. C and D was related to the actual amount of adsorbed  $\text{CO}_2$ , which enabled obtaining the mass of adsorbed  $\text{CO}_2$  through the ratio of the number of moles to the molar mass of carbon dioxide (40.1 g/mol). Therefore, the maximum amount of  $\text{CO}_2$  adsorption was obtained by:

$$q_e = \frac{m_{\text{CO}_2\text{ads}}}{m_{\text{ads}}} \quad (\text{J})$$

in which  $q_e$  is the amount adsorbed,  $m_{\text{CO}_2\text{ads}}$  is the mass of adsorbed  $\text{CO}_2$  (g), and  $m_{\text{ads}}$  is the mass of adsorbent (g).

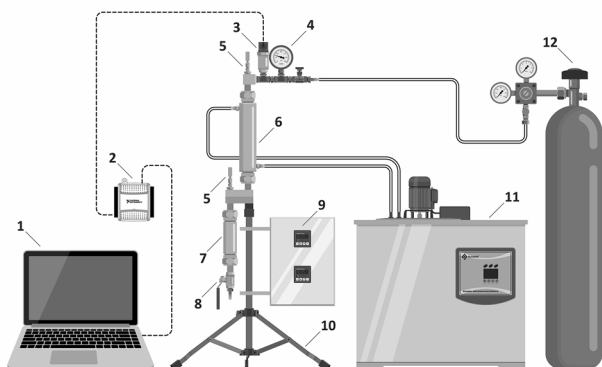


Figure 1: Scheme showing the system used for  $\text{CO}_2$  adsorption tests: 1) workspace created for data acquisition using Matlab/Simulink software; 2) data acquisition board (USB-6008, National Instr.); 3) pressure transmitter (VKP-011, Velki) with measurement capacity from 0 to 0.2 MPa; 4) Bourdon pressure gauge (ASTA) with a pressure range from 0 to 0.1 MPa; 5) PT-100 in stainless steel (1/8" NPT, Ecil) for measuring the temperature in the bed and in the reservoir; 6) stainless steel column (ANSI 304) coupled with a thermal jacket with inlet and outlet for bed temperature control; 7) stainless steel 'lung' type reservoir (ANSI 304); 8) valve for depressurizing the column; 9) temperature display; 10) stainless steel tripod; 11) ultra-thermostatic bath (Quimis); 12) 99%  $\text{CO}_2$  cylinder (White Martins).

*Effect of contact time on the  $\text{CO}_2$  adsorption kinetics:* the effect of the contact time was tested in triplicate using initial pressure ranging from 0.05 to 0.36 MPa, adsorbent mass of 1 g, temperature of 25 °C, and contact time varying between 1 and 60 min. The experimental data were used to determine the kinetic constants according to the pseudo-first-order (Eq. K) and pseudo-second-order (Eq. L) models [16]:

$$q_t = q_e(1 - e^{-k_1 t}) \quad (\text{K})$$

$$q_t = \frac{q_e^2 K_2 t}{1 + q_2 K_2 t} \quad (\text{L})$$

in which  $q_t$  (mg/g) represents the amount adsorbed at time

$t$ ,  $q_e$  is the amount adsorbed at equilibrium (mg/g), and  $k_1$  ( $\text{min}^{-1}$ ) and  $k_2$  ( $\text{g} \cdot \text{mg}^{-1} \cdot \text{min}^{-1}$ ) represent the pseudo-first-order and pseudo-second-order speed constants.

*Effect of initial pressure on the  $\text{CO}_2$  adsorption at equilibrium:* the equilibrium experiments were carried out in triplicates using 1 g of adsorbent mass at 25 °C, 1 h of contact time, and initial  $\text{CO}_2$  pressure varying from 0.05 to 0.36 MPa. The experimental results were used to estimate the maximum adsorbent capacity and possible adjustments to the Langmuir (Eq. M) and Freundlich (Eq. N) models [17]:

$$q_e = \frac{q_{\text{max}} k_L P_e}{1 + k_L P_e} \quad (\text{M})$$

$$q_e = k_F P_e^{1/n} \quad (\text{N})$$

in which  $q_{\text{eq}}$  (mg/g) is adsorbed quantity in the solid phase in equilibrium with the fluid phase at a pressure  $P$ ,  $q_{\text{max}}$  (mg/g) is the maximum adsorption capacity,  $P_e$  (MPa) is the equilibrium pressure,  $k_L$  is the Langmuir constant ( $\text{MPa}^{-1}$ ),  $k_F$  is the Freundlich constant [ $\text{mg}/(\text{g} \cdot \text{MPa}^n)$ ], and  $n$  is the Freundlich equilibrium constant. The  $1/n > 1$  is indicative of cooperative adsorption, while  $0 < 1/n < 1$  adsorption is considered chemical, favorable, and non-linear; the closer to 0, the more heterogeneous the surface [17].

*LTA zeolite regeneration cycles:* the regeneration of LTA zeolite impregnated with  $\text{CO}_2$  after adsorption was carried out using heat treatment (100 °C for 1 h in an oven). After regeneration, the adsorbent was reused under the same conditions as the first cycle to observe the variation in the amount of  $\text{CO}_2$  adsorbed over four additional cycles.

*Estimation of kinetic and equilibrium parameters:* the parameters of kinetics and chemical equilibrium of adsorption were estimated using Statistica 8.0 software and GAMS (general algebraic modeling system) with CONOPT solver with non-linear mathematical programming (NLP) to minimize the sum of squares for error (SSE) objective function (Eq. O). Identification of the best model for adjusting the kinetic and equilibrium models was made using the mean relative error (MRE) discriminator function [17].

$$F_{\text{obj}} = \sum_{i=1}^n (q_{e,\text{calc}} - q_{e,\text{exp}})^2 \quad (\text{O})$$

in which  $n$  is the number of experiments,  $q_{e,\text{calc}}$  is the amount of  $\text{CO}_2$  adsorbed by the mathematical model, and  $q_{e,\text{exp}}$  is the adsorbed quantity measured experimentally.

## RESULTS AND DISCUSSION

The main inorganic constituents of the PIN clay were  $\text{SiO}_2$  and  $\text{Al}_2\text{O}_3$  species as well as  $\text{CaO}$  and  $\text{Fe}_2\text{O}_3$  (Table I). Since the high levels of calcium and iron present in the PIN clay could interfere with the LTA zeolite synthesis [9], the calcium and iron contents were reduced by 97.94% and 82.68%, respectively, using acid treatment. The acid-treated

Table I - Inorganic chemical composition (%w/w) of natural (PIN) and modified (PIN-MOD) clays.

Component	PIN clay	PIN-MOD clay
SiO <sub>2</sub>	56.02	75.85
Al <sub>2</sub> O <sub>3</sub>	18.88	15.67
CaO	8.26	0.17
Fe <sub>2</sub> O <sub>3</sub>	7.45	1.29
K <sub>2</sub> O	3.32	3.26
MgO	3.26	1.09
Na <sub>2</sub> O	1.46	1.61
TiO <sub>2</sub>	0.96	0.96
P <sub>2</sub> O <sub>5</sub>	0.18	-
BaO	0.09	0.08
MnO	0.06	-
ZrO <sub>2</sub>	0.03	0.02
ZnO	0.02	-
SrO	0.01	-
Total	100.00	100.00

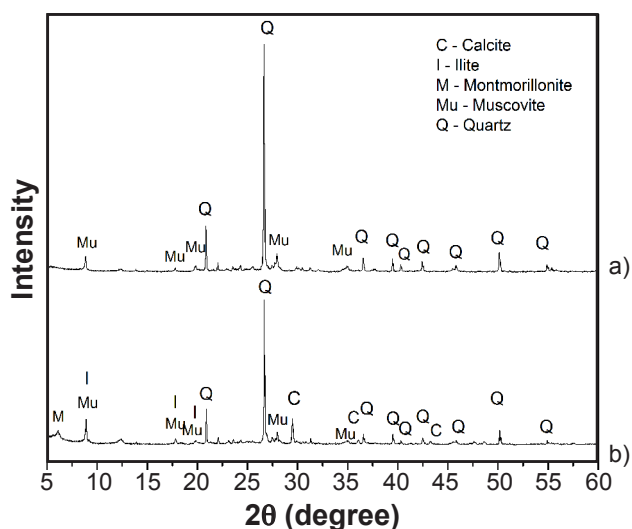


Figure 2: X-ray diffractograms for PIN clay (a) and PIN-MOD clay (b).

PIN clay (PIN-MOD clay) was composed mostly of silica and alumina and was suitable for the production of LTA zeolite. The fraction of organic matter and the amount of exchangeable cations also decreased after acid treatment. The fraction of organic matter dropped from 1.76% in the PIN clay to 1.25% in the PIN-MOD clay, while the amount of exchangeable cations (measured by the CTC analysis) went down from 6.33 cmol/kg in the PIN clay to 3.94 cmol/kg for PIN-MOD clay. Fig. 2 shows the diffractograms of the PIN and PIN-MOD clays. The main crystalline phases in the PIN clay were quartz (SiO<sub>2</sub>), muscovite [KAl<sub>2</sub>(AlSi<sub>3</sub>O<sub>10</sub>)(F,OH)<sub>2</sub>], illite {(K,H<sub>3</sub>O)(Al,Mg,Fe)<sub>2</sub>(Si,Al)<sub>4</sub>O<sub>10</sub>[(OH)<sub>2</sub>,H<sub>2</sub>O]}, montmorillonite [(Mg,Ca)O·Al<sub>2</sub>O<sub>3</sub>·Si<sub>3</sub>O<sub>10</sub>·nH<sub>2</sub>O] and

calcite (CaCO<sub>3</sub>), whereas calcite, illite, and montmorillonite phases were not present in the PIN-MOD clay. The decrease in the concentration of calcium (present in calcite and montmorillonite), iron, aluminum, and magnesium (present in illite and montmorillonite) indicated a change in the crystalline structure caused by the weakening of chemical bonds via thermochemical reactions during acid treatment [18].

The effect of different calcination times (2, 4, and 6 h, followed by 4 h of hydrothermal treatment at 100 °C) on the synthesis of LTA zeolite can be observed in Fig. 3. For example, the presence of high-intensity quartz and alumina peaks in the XRD diffractogram of the product obtained after 2 h of calcination indicated that insufficient energy was provided to weaken and break the crystalline structure bonds of the PIN clay. In this case, a possible increase in the reactive SiO<sub>2</sub>/Al<sub>2</sub>O<sub>3</sub> ratio favored the formation of zeolite X instead of LTA zeolite [19]. It was possible to obtain the LTA zeolite after 4 and 6 h of calcination without simultaneous formation of other zeolitic structures, with the samples showing 42.72% crystallinity at 4 h and 71.60% at 6 h compared to the LTA-standard zeolite. LTA-standard zeolite prepared by the conventional route was confirmed by the XRD pattern regulated by IZA [5]. These results showed that calcination time greatly affected the formation of LTA zeolite. Quartz from the PIN-MOD clay was still present in the synthesized LTA zeolite. Similarly, it was also observed in the literature the presence of quartz in the LTA zeolite when using fly ash as starting material [20].

Fig. 4 shows that the hydrothermal treatment time affected the crystallinity of the LTA zeolite. Increasing the hydrothermal treatment time from 3 to 4 h raised the crystallinity from 63.88% to 71.60%. However, a further increase of hydrothermal treatment time to 6 h led to a decrease in the crystallinity of the LTA zeolite produced (63.24%). It should be noted that the LTA-PIN zeolite with the highest crystallinity (71.60%) was synthesized using the

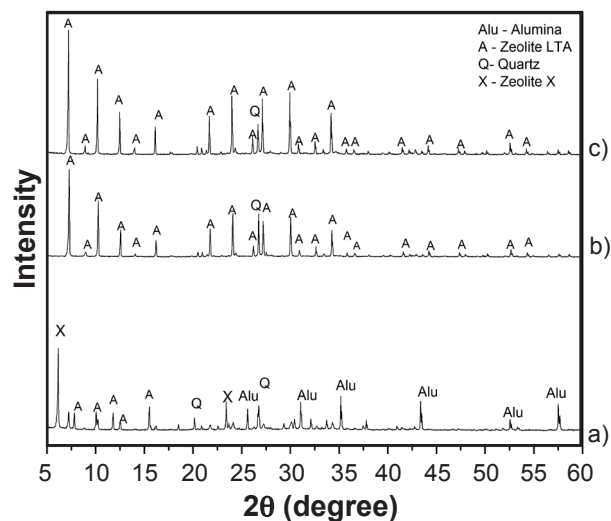


Figure 3: X-ray diffractograms of LTA zeolite obtained with 2 h (a), 4 h (b), and 6 h (c) of calcination treatment at 600 °C followed by 4 h of hydrothermal treatment at 100 °C.

same hydrothermal treatment time (4 h) described by IZA [5] using the conventional route. Based on these results, the experimental conditions leading to the highest crystallinity (calcination for 6 h followed by 4 h of hydrothermal treatment) were selected for the production of the zeolite, which is simply referred to as LTA-PIN zeolite in the remainder of the article and was used for all tests presented from this point forward.

In addition to calculating the crystallinity degree using the intensity of the main peaks, the LTA-PIN zeolite and LTA-standard zeolite diffractograms (Fig. 5) were refined using the crystallographic pattern available in the IZA database for the structure of the LTA zeolite. The results showed that LTA-PIN zeolite was composed of 95.70% of the LTA phase (with a composition of  $\text{Na}_{62}\text{Si}_{96}\text{Al}_{96}\text{O}_{692}$ ) and 4.30% of quartz ( $\text{SiO}_2$ ), while the LTA-standard zeolite presented 100% of the LTA phase with a

composition of  $\text{Na}_{58}\text{Si}_{96}\text{Al}_{96}\text{O}_{696}$ . Both zeolites showed low sodium deficiency in the structure when compared to the theoretical composition of  $\text{Na}_{64}\text{Si}_{96}\text{Al}_{96}\text{O}_{710}$  [5]. This observation indicated the formation of intercrystals during hydrothermal treatment since the charge compensator (Na in LTA zeolite) occupies the central part of the structure [21]. Despite the presence of remaining quartz, the LTA-PIN zeolite did not show a deficiency of silica in its crystalline structure, indicating that the reaction mixture had the appropriate reactive composition to obtain the LTA zeolite. Table II shows that the main components of the LTA-PIN zeolite were  $\text{SiO}_2$ ,  $\text{Al}_2\text{O}_3$ , and  $\text{Na}_2\text{O}$ . Similar amounts of these components were found in the LTA-standard zeolite. Other components present in the PIN-MOD clay were also found in quantities below 1% in the LTA-PIN zeolite. These quantities were very low to affect the formation of the LTA-PIN zeolite.

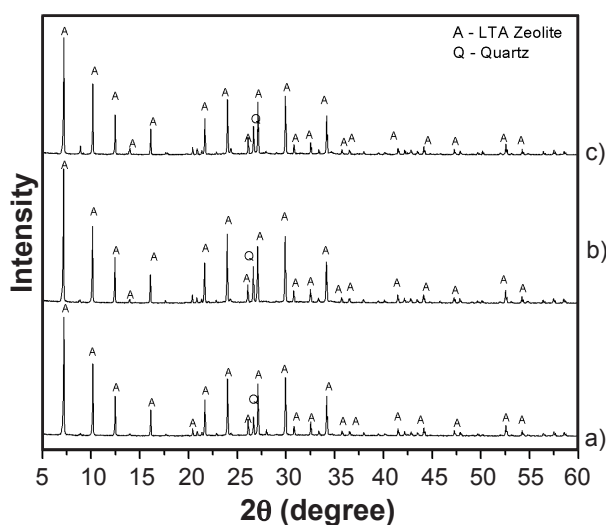


Figure 4: X-ray diffractograms of LTA zeolite obtained with 6 h of calcination and hydrothermal treatment for 3 h (a), 4 h (b), and 6 h (c) at 100 °C.

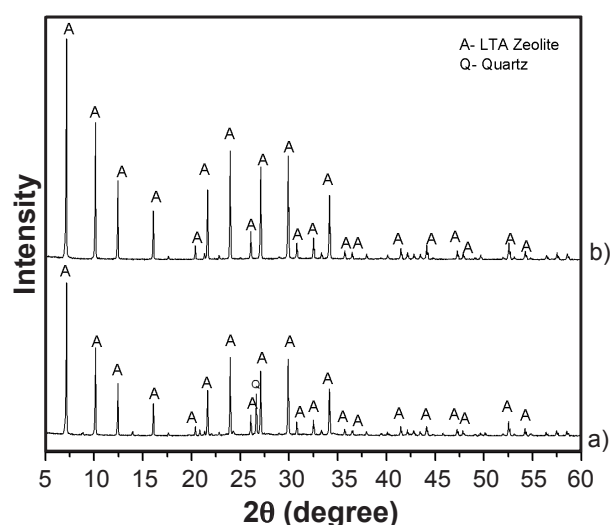


Figure 5: X-ray diffractograms for LTA-PIN zeolite (a) and LTA-standard zeolite (b).

Table II - Inorganic chemical composition of LTA-PIN zeolite and LTA-standard zeolite.

Component	LTA-PIN zeolite (%w/w)	LTA-standard zeolite (%w/w)	LTA-PIN zeolite (mol)	LTA-standard zeolite (mol)
$\text{SiO}_2$	41.26	39.27	2.1525	1.9019
$\text{Al}_2\text{O}_3$	32.53	35.04	1.0000	1.0000
$\text{Na}_2\text{O}$	23.36	25.67	1.1815	1.2053
$\text{K}_2\text{O}$	0.88	-	0.0293	-
$\text{Fe}_2\text{O}_3$	0.72	0.03	0.0141	0.0004
$\text{TiO}_2$	0.59	-	0.0231	-
$\text{MgO}$	0.48	-	0.0373	-
$\text{CaO}$	0.11	-	0.0061	-
$\text{BaO}$	0.05	-	0.0010	-
$\text{ZrO}_2$	0.01	-	0.0002	-
Total	100.00	100.00		

The main functional groups characteristic of the clays and zeolites were identified by FTIR (Fig. 6). The PIN clay and PIN-MOD clay spectra presented characteristic bands at 3455  $\text{cm}^{-1}$ , attributed to the vibrations of the hydroxyl groups of water molecules, in addition to angular deformation for the adsorbed water molecules identified in 1648  $\text{cm}^{-1}$  [22, 23]. The band at 3621  $\text{cm}^{-1}$  was attributed to the structural -OH [23]. The 1421  $\text{cm}^{-1}$  adsorption band in the PIN clay attributed to the stretching vibrations of the  $\text{CO}_3^{2-}$  ion (from calcite) disappeared after the acid treatment due to the reaction with HCl, thereby forming  $\text{CO}_2$  and  $\text{H}_2\text{O}$  [23]. The bands at 1027, 798, and 470  $\text{cm}^{-1}$  associated with the asymmetric Si-O-Si stretching vibrations [24-26] became wider and less intense after acid treatment, indicating the weakening of these bonds and the formation of less crystalline material. The shoulder at 910  $\text{cm}^{-1}$  was attributed to Al-OH connections, while the band at 696  $\text{cm}^{-1}$  was associated with Al-O-Al vibrations [23]. The 873  $\text{cm}^{-1}$  band in the PIN clay spectrum was attributed to the Fe-OH stretching vibrations [25] and disappeared after the acid treatment, indicating a rupture of the bonds involving the iron. This conclusion was supported also by the XRD (which showed the disappearance of illite) and XRF (which showed a decrease in the iron content of the clay) results. Other bands at 669, 557, 445, and 410  $\text{cm}^{-1}$  in the adsorption region of metallic bonds [24] also disappeared after acid treatment and were related to the bonds of the metallic cations present in the PIN clay. The LTA zeolite main adsorption bands were located at 3467  $\text{cm}^{-1}$  (related

to the -OH stretching), 1658  $\text{cm}^{-1}$  (attributed to the H-O-H angular deformation), 1012  $\text{cm}^{-1}$  (attributed to the Si-O-Si vibration), 669  $\text{cm}^{-1}$  (related to the vibration of the sodalite structure ring), 557  $\text{cm}^{-1}$  (attributed to bicyclic vibrations in a tetrahedral structure), and 462  $\text{cm}^{-1}$  (referring to TO vibrations, T being Si or Al) [27, 28]. The LTA-PIN zeolite and LTA-standard zeolite had similar FTIR spectra, with both materials presenting the same functional groups. These observations were in agreement with the reorganization of the crystalline structure observed in the XRD analyzes.

SEM micrographs showed the PIN clay morphology, which consisted of stacked flakes organized in agglomerates (Fig. 7a). After the acid treatment, the PIN-MOD clay (Fig. 7b) had a smaller amount of agglomerated flakes, which was attributed to the absence of the calcite and illite phases, in agreement with the XRD results. The reorganization of the crystalline structure of the PIN-MOD clay during hydrothermal treatment was visually confirmed in the micrograph of the LTA-PIN zeolite (Fig. 7c), which had a well-defined cubic structure. A similar cubic structure was also observed for the LTA-standard zeolite (Fig. 7d) [21, 28]. The formation of intercrystals observed in the LTA-PIN zeolite and LTA-standard zeolite micrographs was probably caused by the absence of agitation during the hydrothermal treatment [21, 27].

Fig. 8 shows the  $\text{N}_2$  physisorption isotherms for the PIN clay, PIN-MOD clay, LTA-PIN zeolite, and LTA-standard zeolite samples. Table III shows the specific surface area values calculated using the BET method. It was possible to

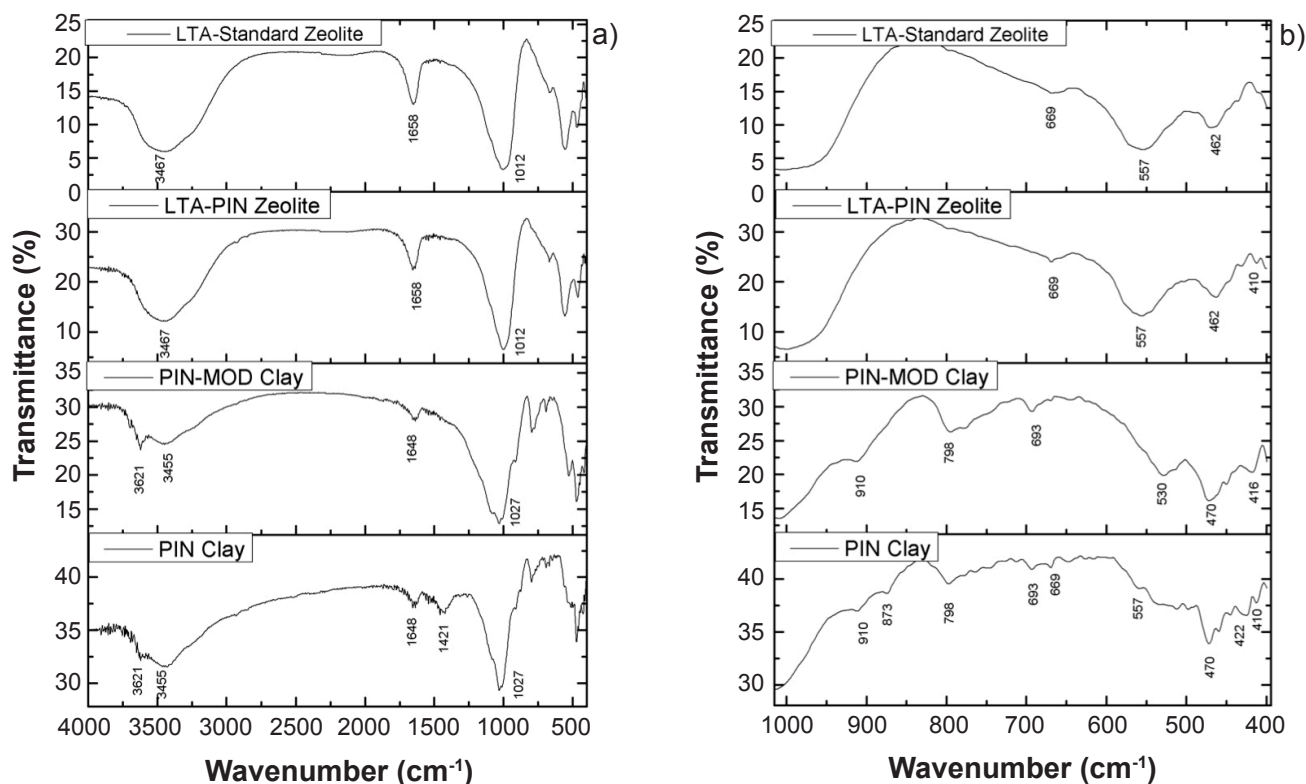


Figure 6: FTIR spectra of PIN clay, PIN-MOD clay, LTA-PIN zeolite, and LTA-standard zeolite: a) full spectrum; and b) region between 100 and 400  $\text{cm}^{-1}$ .

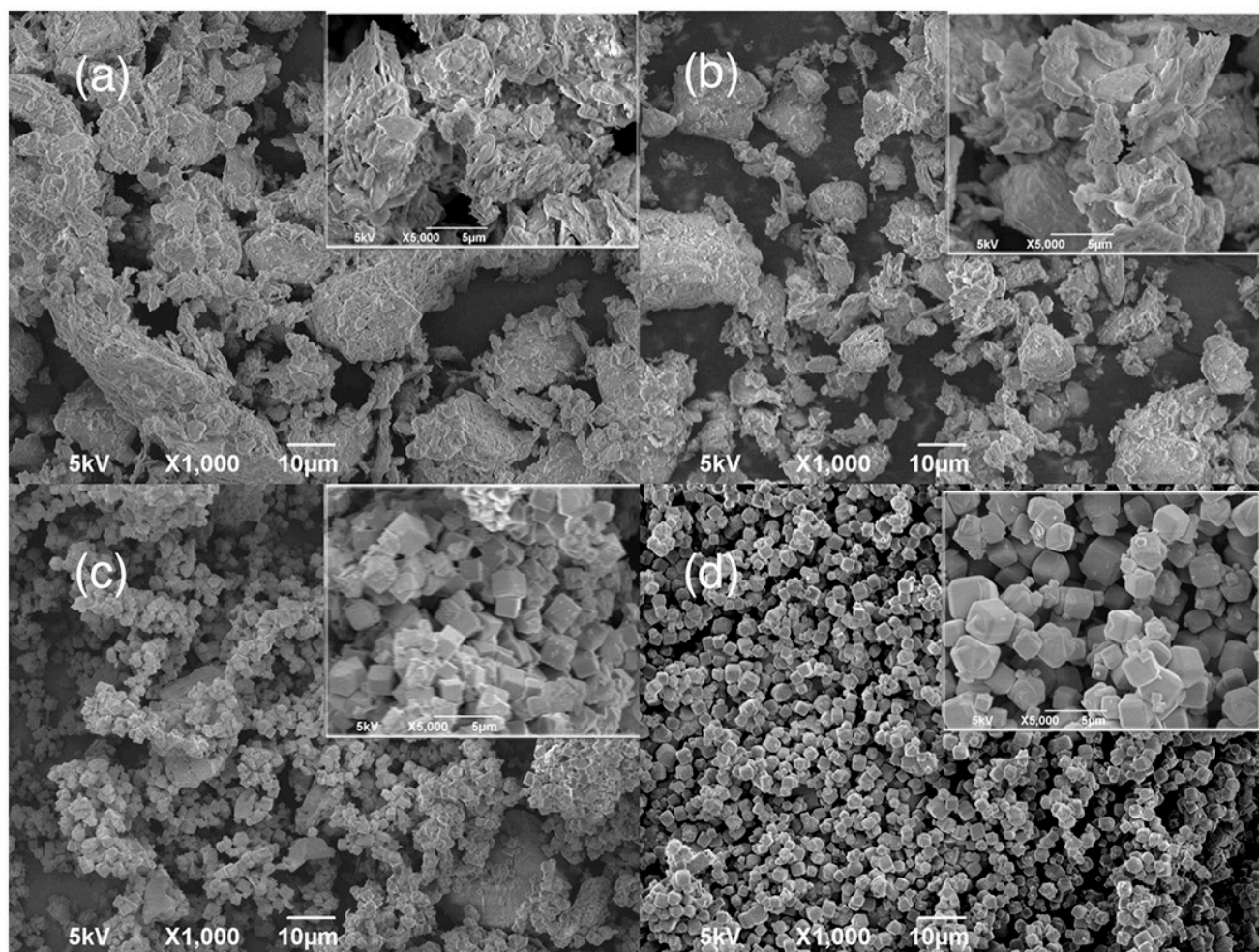


Figure 7: Scanning electron micrographs of: a) PIN clay; b) PIN-MOD clay; c) LTA-PIN zeolite; and d) LTA-standard zeolite.

observe an increase in the surface area of the clay after the acid treatment due to the removal of impurities and cations from the crystalline structures [23]. However, both the LTA-PIN zeolite and LTA-standard zeolite had a significantly lower surface area compared to the PIN and PIN-MOD clays. The lower surface area can be attributed to the narrow pore opening of the LTA structure and the kinetic restriction of the diffusion of  $N_2$  at 77 K; such characteristics make it impossible to obtain values with physical meaning [29-31]. The characterization analyzes allowed to observe the structural change of the PIN clay and through the acid, thermal, and hydrothermal treatments, the crystalline restructuring and obtaining of the LTA-PIN zeolite was proven. Before concluding the characterization step, it is important to report that the characterization of adsorbents after solid-gas adsorption was limited due to the different conditions of pressure and temperature during the experiment and the characterization analysis (which needed previous heat treatment). This deficient knowledge of the molecular-level interactions and their effect on macroscopic phenomena, as described by Roque-Malherbe [15], was also observed in other reported studies involving the adsorption of  $CO_2$  in zeolites [29-31].

A preliminary adsorption test was carried out to

determine the amount of  $CO_2$  adsorbed by the PIN and PIN-MOD clays as well as LTA-PIN zeolite and LTA-standard zeolite (Eqs. C to J). This adsorption test used the volume

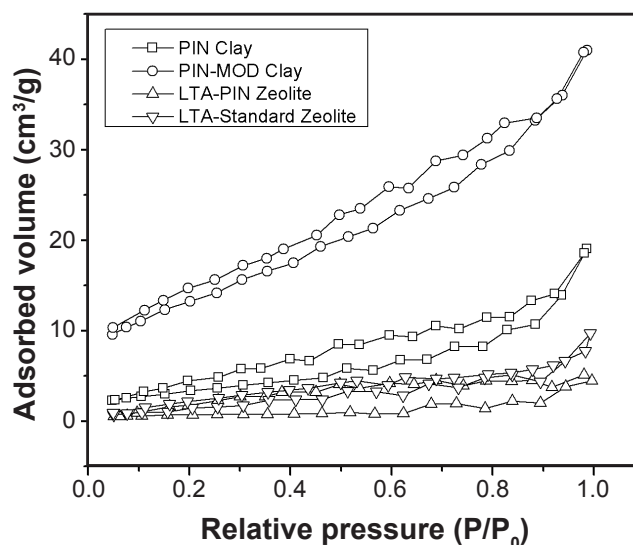


Figure 8:  $N_2$  adsorption/desorption isotherms for PIN and PIN-MOD clays and LTA-PIN and LTA-standard zeolites.

Table III - Specific surface area (BET) determined by nitrogen gas physisorption and density of clays and zeolites.

Material	BET specific area (m <sup>2</sup> /g)	Density (g/cm <sup>3</sup> )
PIN clay	12.47	2.7810±0.0018
PIN-MOD clay	48.33	2.7342±0.0020
LTA-PIN zeolite	2.30	2.0457±0.0008
LTA-standard zeolite	6.08	2.0638±0.0031

occupied by the CO<sub>2</sub> and the adsorbent inside a fixed volume column (138.54 cm<sup>3</sup>) to calculate the amount of adsorbed CO<sub>2</sub>. In this case, it was necessary to determine the density of the adsorbent materials to calculate the volume occupied by the adsorbent and to correct the volume occupied by CO<sub>2</sub> in the adsorption column (Eqs. A and B). Table III shows that the clays (PIN and PIN-MOD) had greater densities compared to the zeolites (LTA-PIN and LTA-standard). In the end, the amount of CO<sub>2</sub> adsorbed was calculated using the input data presented in Table IV and Eqs. A to J [32]. The amount of CO<sub>2</sub> adsorbed by the clay doubled after acid treatment (Table V), increasing from 2.29 mg/g for the PIN clay to 4.6 mg/g for the PIN-MOD clay. This behavior can be associated with the higher surface area of the PIN-MOD clay. However, the CO<sub>2</sub> adsorptive capacities of PIN and PIN-MOD clays were really low when compared to the ones of LTA-PIN zeolite and LTA-standard zeolite (63.64 and 31.66 mg/g, respectively). The lower adsorption capacity of the PIN and PIN-MOD clays can be attributed to the weak physical interaction between CO<sub>2</sub> and the external surface of the clays [33]. The CO<sub>2</sub> adsorption on LTA zeolite took place inside the pores that had a 4.1 Å aperture diameter for the sodium structure allowing the entry of CO<sub>2</sub> molecules, which had a kinetic diameter of 3.3 Å [34]. Based on these preliminary results, further CO<sub>2</sub> adsorption experiments and kinetic studies were performed using only the LTA-PIN zeolite and the LTA-standard zeolite.

The kinetic study and determination of kinetic parameters allowed us to evaluate the CO<sub>2</sub> adsorption process, especially with respect to maximum CO<sub>2</sub> adsorption capacity, which can be estimated using CO<sub>2</sub> quantity adsorbed at equilibrium. The kinetic parameters of an adsorbent evaluated in a static system is an important step for process design and optimization in dynamic systems as technology moves towards industrial process application [15]. Fig. 9a presents the amount of CO<sub>2</sub> adsorbed into LTA-PIN zeolite and the LTA-standard zeolite as a function of time for an initial pressure of 0.26 MPa. The graph shows that CO<sub>2</sub> adsorption progressed rapidly for both zeolite structures in the first 20 min when the difference in the CO<sub>2</sub> concentration in the fluid and solid phases was greater. Fast CO<sub>2</sub> adsorption at the beginning of the adsorption experiment suggested a high affinity between CO<sub>2</sub> and the zeolites [29]. Equilibrium was reached after 40 min for the LTA-PIN zeolite and 20 min for the LTA-standard zeolite. After 60 min, the amount of adsorbed CO<sub>2</sub> was 90.67 and

Table IV - Constants and parameters used to calculate (according to Eqs. A to J) the amount of CO<sub>2</sub> adsorbed during CO<sub>2</sub> adsorption tests.

Property	Value	Unit
Critical temperature (T <sub>c</sub> )	304.2	K
Critical pressure (P <sub>c</sub> )	7.832	MPa
Critical volume (V <sub>c</sub> )	94.8	cm <sup>3</sup> /mol
Compressibility factor (z)	0.277	-
Acentric factor (ω)	0.239	-
Gas constant (R)	8.314	cm <sup>3</sup> .MPa/K

Table V - Amount of CO<sub>2</sub> adsorbed (mg/g) into different clays and zeolites during the CO<sub>2</sub> adsorption test, which was performed for 1 h at 25 °C and using initial pressure of 0.1 MPa.

PIN clay	PIN-MOD clay	LTA-PIN zeolite	LTA-standard zeolite
2.29±0.83	4.60±0.14	63.64±1.79	31.66±0.68

96.01 mg/g for LTA-PIN zeolite and LTA-standard zeolite, respectively. The experimental data were used to calculate the kinetic parameters for the pseudo-first-order and pseudo-second-order models (Eqs. K and L). According to these results (Table VI and Fig. 9a), the kinetic models used were able to predict the behavior of CO<sub>2</sub> access to the zeolite pores throughout the adsorption process. The pseudo-second-order model was the best fit for the experimental data of the LTA-PIN zeolite and the LTA-standard zeolite, as indicated by the smallest error in the parameters and the highest coefficient of determination obtained for this model. The main assumption of the pseudo-second-order kinetic model is that the rate of adsorption is proportional to the square of the number of free active sites at the adsorbent surface [16]. The other two kinetic parameters, the velocity constant (k<sub>2</sub>) and amount of CO<sub>2</sub> adsorbed at equilibrium (q<sub>e</sub>), obtained with the pseudo-second-order model (Table VI) indicated that CO<sub>2</sub> adsorption was significantly faster in the case of the LTA-standard zeolite, which presented a rate constant of 0.0037 g/(mg.min). However, a larger amount of CO<sub>2</sub> was adsorbed into the LTA-PIN zeolite structure (q<sub>e</sub>=101.26 mg/g) compared to the amount adsorbed by the LTA-standard zeolite (q<sub>e</sub>=95.53 mg/g).

Additional equilibrium experiments were carried out to estimate the maximum adsorption capacity of the adsorbents. Fig. 9b displays the amount of CO<sub>2</sub> adsorbed as a function of the equilibrium pressure. The plot shows that the amount of CO<sub>2</sub> adsorbed by the LTA-PIN zeolite was higher than the one adsorbed by the LTA-standard zeolite in the pressure region ranging between 0.05 and 0.20 MPa. However, the amount of CO<sub>2</sub> adsorbed by the LTA-PIN zeolite started to level off when pressure was raised above 0.20 MPa, indicating that the LTA-PIN zeolite reached its maximum CO<sub>2</sub> adsorption capacity. On the other hand, saturation was

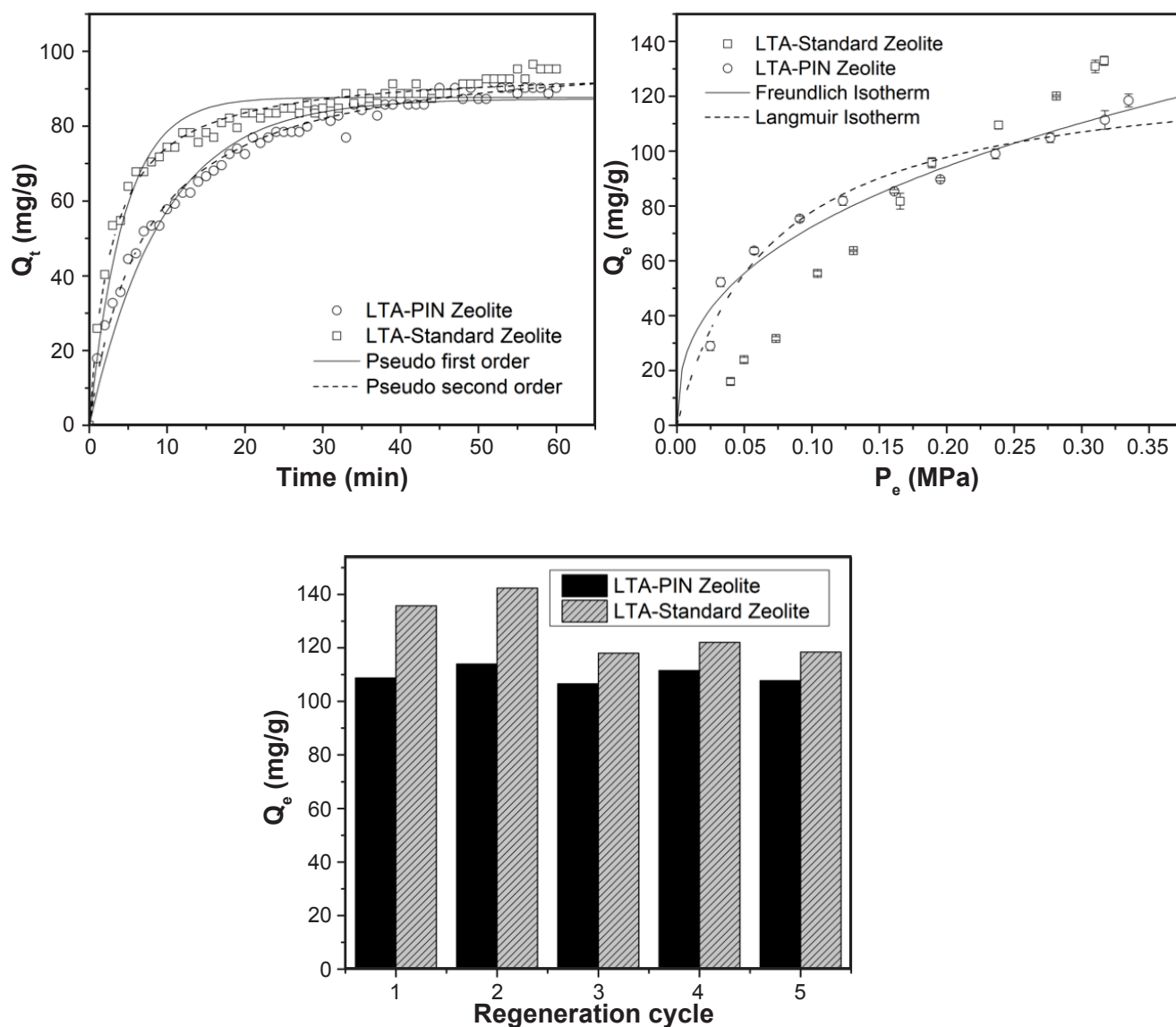


Figure 9: Results of adsorption study: a) kinetics curves and amount of CO<sub>2</sub> adsorbed by LTA-PIN and LTA-standard zeolites versus time using 1 g of adsorbent, 25 °C, an initial pressure of 0.26 MPa, and contact time between 1 and 60 min; b) kinetics curves and amount of adsorbed CO<sub>2</sub> in the solid phase in equilibrium with the fluid phase versus equilibrium pressure for the zeolites under the experimental conditions of 25 °C, for 1 h at pressures between 0.05 and 0.36 MPa; c) five adsorption/desorption cycles for zeolites: regeneration was achieved using heat treatment (100 °C for 1 h); after regeneration, the adsorbent was reused for CO<sub>2</sub> adsorption at an initial pressure of 0.36 MPa.

not reached in the case of the LTA-standard zeolite even when the pressure was increased from 0.2 to 0.35 MPa, indicating that free sites in the LTA-standard zeolite were still available for CO<sub>2</sub> retention. Fig. 9b also shows the adjustment of the Langmuir (Eq. M) and Freundlich (Eq. N) isotherm models to the experimental data. Table VII presents the estimated parameters for these models. The results showed that in both models the adjustment of the correlation coefficient was  $r^2 > 0.9$ . The experimental data of the LTA-PIN zeolite were better predicted by the Freundlich model. The best fit to the Freundlich model indicated that the adsorption of CO in the pores of the zeolite LTA-PIN occurred mainly through physical interactions with the electric field generated by the charges [35, 36].

Table VIII shows the comparison of the CO<sub>2</sub> adsorptive capacities for different materials at very low CO<sub>2</sub> pressure (0.1 MPa). The LTA-PIN zeolite had twice the adsorption capacity of the LTA-standard zeolite and was more efficient than activated carbon and other clays at the same experimental conditions, demonstrating the commercial potential of the LTA-PIN zeolite for CO<sub>2</sub> adsorption applications. The regeneration study was performed to determine the possibility of zeolite reuse. Fig. 9c shows that the LTA-PIN zeolite had a low loss of CO<sub>2</sub> adsorption capacity after 5 adsorption/desorption cycles (at an initial pressure of 0.036 MPa), suggesting that LTA-PIN zeolite can be potentially reused. Despite having a higher initial CO<sub>2</sub> adsorption capacity, the LTA-standard zeolite showed

Table VI - Kinetic models and their respective parameters obtained in the study of CO<sub>2</sub> adsorption by LTA-PIN zeolite and LTA-standard zeolite using 1 g of adsorbent, 25 °C, and initial pressure of 0.26 MPa.

Parameter	LTA-PIN	LTA-standard
Pseudo-first-order		
q <sub>e,cal</sub> (mg/g)	87.3±0.7	87.7±0.7
k <sub>1</sub> (min <sup>-1</sup> )	0.107±0.004	0.226±0.013
r <sup>2</sup>	0.9668	0.9214
Mean error	0.0534	0.0543
Pseudo-second-order		
q <sub>e,cal</sub> (mg/g)	101.3±0.7	95.5±0.5
k <sub>2</sub> (g.mg <sup>-1</sup> .min <sup>-1</sup> )	0.0014±0.0001	0.0037±0.0002
r <sup>2</sup>	0.9906	0.9820
Mean error	0.0266	0.0225

Table VII - Kinetic models and their respective parameters obtained in the study of CO<sub>2</sub> adsorption equilibrium using 1 g of adsorbent, 25 °C, and initial pressure of 0.26 MPa.

Parameter	LTA-PIN zeolite	LTA-standard zeolite
Langmuir		
q <sub>max</sub> (mg/g)	131±7	546±123
k <sub>L</sub> (MPa <sup>-1</sup> )	14.53±2.55	1.03±0.29
r <sup>2</sup>	0.9484	0.9916
Mean error	0.0727	0.0803
Freundlich		
K <sub>F</sub> (mg.g <sup>-1</sup> .MPa <sup>-n</sup> )	175±10	368±25
n	2.61±0.03	1.16±0.04
r <sup>2</sup>	0.9558	0.9870
Mean error	0.0819	0.0977

Table VIII - Comparison of the amount of CO<sub>2</sub> adsorbed by different adsorbents after 1 h at 25 °C and 0.1 MPa.

Adsorbent	Amount of CO <sub>2</sub> adsorbed (mg/g)	Ref.
PIN clay	2.29	This work
PIN-MOD clay	4.60	This work
Acid-treated bentonite	25.78	[37]
Modified activated carbon	50	[38]
Activated carbon	45	[14]
Sod-ZMOF	53	[39]
LTA-PIN zeolite	63.64	This work
LTA-standard zeolite	31.66	This work

a 12.76% reduction in adsorptive capacity after five cycles, indicating that part of the sites became inaccessible after the adsorption/desorption cycles.

## CONCLUSIONS

LTA zeolite was obtained (LTA-PIN zeolite) using Pinheiro clay (PIN clay). The LTA zeolite produced can potentially be used for CO<sub>2</sub> adsorption applications. Pinheiro clay from the State of Sergipe (Brazil) was successfully converted into LTA zeolite using acid, calcination, and hydrothermal treatments during the synthesis process. The acid treatment was efficient in purifying clay, making it more susceptible to recrystallization to obtain the LTA zeolite. The calcination and hydrothermal treatment time were influential in the synthesis process, with higher crystallinity and purity zeolite (71.60% and 95.79%, respectively) being obtained with 6 h of calcination and 4 h of hydrothermal treatment. XRD results confirmed that, before treatments, the main crystalline phases of the Pinheiro clay were muscovite, illite, calcite, montmorillonite, and quartz, whereas, after the treatments, the main crystalline phase of the synthesized LTA-PIN zeolite was the LTA phase (95.70%). In addition, CO<sub>2</sub> adsorption tests revealed that the majority of the CO<sub>2</sub> adsorption occurred in less than 30 min at low pressure (0.26 MPa) for both the LTA-PIN zeolite and the LTA-standard zeolite. At the end of the test (1 h), similar amounts of CO<sub>2</sub> were captured by the LTA-PIN and LTA-standard zeolites (90.67 and 96.01 mg/g, respectively). However, the LTA-PIN zeolite performance was significantly higher than LTA-standard zeolite at low CO<sub>2</sub> pressure (0.1 MPa). In this case, LTA-PIN zeolite could retain twice the amount of CO<sub>2</sub> recovered by the LTA-standard zeolite (63.64 and 31.66 mg/g, respectively). At the same time, LTA-PIN zeolite was also more efficient than activated carbon and other modified clays typically used for CO<sub>2</sub> capture under the same experimental conditions. It is important to highlight that LTA-PIN zeolite can be reused up to 5 times without loss of CO<sub>2</sub> adsorption capacity according to the regeneration study results. In contrast, the LTA-standard zeolite showed a loss of 12.76% in adsorptive capacity after five regeneration cycles. Kinetic and isotherm models (pseudo-first-order, pseudo-second-order, Langmuir, and Freundlich models) were used to increase the understanding of the kinetics of the CO<sub>2</sub> adsorption process and estimate the maximum CO<sub>2</sub> adsorption capacity, which can be obtained using the CO<sub>2</sub> quantity adsorbed at equilibrium. The pseudo-second-order kinetic and Freundlich isotherm models best represented the CO<sub>2</sub> adsorption by the LTA-PIN zeolite during the contact time experiments (at 0.26 MPa for 1-60 min) and equilibrium experiments (1 h at 0.05-0.36 MPa), respectively. The equilibrium results suggested that the physical adsorption was the main mechanism responsible for CO<sub>2</sub> adsorption by the zeolites being predicted by the Freundlich model representing physical interactions between CO<sub>2</sub> and charge compensators of LTA-PIN zeolite. In summary, the results reported (especially CO<sub>2</sub> adsorption capacity and

regeneration capacity) indicated that LTA-PIN zeolite has the potential to be commercially explored, increasing the value of the abundantly available PIN clay.

## ACKNOWLEDGMENTS

The authors would like to thank CAPES (Coordenação de Aperfeiçoamento de Pessoal de Nível Superior, Brazil), FAPITEC-SE, CNPq, and UFS for the financial support. The authors would also like to thank the Laboratory of Nanotechnology and Supercritical Technology of the State University of Maringá (UEM) and LQI-UFS.

## REFERENCES

- [1] Intergovernmental Panel on Climate Change, “Climate change 2014: mitigation of climate change”, Cambridge Un. Press (2015).
- [2] M. Mofarahi, F. Gholipour, Microporous Mesoporous Mater. **200** (2014) 1.
- [3] S.-Y. Lee, S.-J. Park, J. Ind. Eng. Chem. **23** (2015) 1.
- [4] Y. Kalvachev, D. Zgureva, S. Boycheva, B. Barbov, N. Petrova, J. Therm. Anal. Calorim. **124** (2016) 101.
- [5] S. Mintova, “Verified syntheses of zeolitic materials”, 3<sup>rd</sup> ed., Int. Zeolite Ass. (2016).
- [6] G. García, W. Aguilar-Mamani, I. Carabante, S. Cabrera, J. Hedlund, J. Mouzon, J. Alloys Compd. **619** (2015) 771.
- [7] C. Chen, D.W. Park, W.S. Ahn, Appl. Surf. Sci. **292** (2014) 63.
- [8] C.A.F. Rocha Junior, R.S. Angélica, R.F. Neves, Cerâmica **61**, 358 (2015) 259.
- [9] J. Jiang, L. Feng, X. Gu, Y. Qian, Y. Gu, C. Duanmu, Appl. Clay Sci. **55** (2012) 108.
- [10] NBR 6502, “Rochas e solos”, ABNT (1995).
- [11] D 2974-00, “Standard test methods for moisture, ash and organic matter of peat and other organic soils”, ASTM (2011).
- [12] M.M.J. Treacy, Appl. Catal. **21** (1986) 388.
- [13] C 837-0, “Standard test method for methylene blue index of clay”, ASTM (2014).
- [14] P.C.C. Araújo, J.J. Marques, E.D.J. Santos, L. Cardozo Filho, D.R. Gonçalves Júnior, Sci. Plena **14** (2018) 1.
- [15] R.M.A. Roque-Malherbe, *Adsorption and diffusion in nanoporous materials*, Taylor Francis (2007).
- [16] S. Mutyala, M. Jonnalagadda, H. Mitta, R. Gundeboyina, Chem. Eng. Res. Des. **143** (2019) 241.
- [17] K.Y. Foo, B.H. Hameed, Chem. Eng. J. **156** (2010) 2.
- [18] V.A.A. España, B. Sarkar, B. Biswas, R. Rusmin, R. Naidu, Environ. Technol. Innov. **13** (2019) 383.
- [19] Z. Zhang, Y. Xiao, B. Wang, Q. Sun, H. Liu, Energy Procedia **114** (2017) 2537.
- [20] N. Yang, S. Liu, X. Yang, Appl. Surf. Sci. **356** (2015) 1262.
- [21] L. Ayele, J. Pérez-Pariente, Y. Chebude, I. Díaz, Appl. Clay Sci. **132-133** (2016) 485.
- [22] A.E.I. Elkhalfah, M. Azmi Bustam, A.M. Shariff, T. Murugesan, Appl. Clay Sci. **107** (2015) 213.
- [23] A.Y. Sidorenko, A.V. Kravtsova, A. Aho, I. Heinmaa, T.F. Kuznetsova, D.Y. Murzin, V.E. Agabekov, Mol. Catal. **448** (2018) 18.
- [24] N.B. Colthup, L.H. Daly, S.E. Wiberly, *Introduction to infrared and Raman spectroscopy*, 3<sup>rd</sup> ed., Acad. Press, New York (1990).
- [25] A. Ahmed, Y. Chaker, E.H. Belarbi, O. Abbas, J.N. Chotard, H.B. Abassi, A.N. van Nhien, M. El Hadri, S. Bresson, J. Mol. Struct. **1173** (2018) 653.
- [26] J. Yuan, J. Yang, H. Ma, S. Su, Q. Chang, S. Komarneni, Appl. Clay Sci. **165** (2018) 71.
- [27] M. Anbia, E. Koohsaryan, A. Borhani, Mater. Chem. Phys. **193** (2017) 380.
- [28] G. Yang, S. Song, J. Li, Z. Tang, J. Ye, J. Yang, J. Mater. Sci. Technol. **35** (2019) 875.
- [29] C. Chen, W.S. Ahn, Appl. Surf. Sci. **311** (2014) 107.
- [30] R. Seabra, A.M. Ribeiro, K. Gleichmann, A.F.P. Ferreira, A.E. Rodrigues, Microporous Mesoporous Mater. **277** (2019) 105.
- [31] E. Khoramzadeh, M. Mofarahi, C.-H. Lee, J. Chem. Eng. Data **64** (2019) 5648.
- [32] M. Smith, J.M. Van Ness, H.C. Abbott, *Introdução à termodinâmica da engenharia química*, 7<sup>th</sup> ed., LTC (2007).
- [33] C. Chen, D.W. Park, W.S. Ahn, Appl. Surf. Sci. **283** (2013) 699.
- [34] Z. Bacsik, O. Cheung, P. Vasiliev, N. Hedin, Appl. Energy **162** (2016) 613.
- [35] B. Petrovic, M. Gorbounov, S. Masoudi Soltani, Microporous Mesoporous Mater. **312** (2021) 110751.
- [36] D. Panda, E.A. Kumar, S.K. Singh, J. CO<sub>2</sub> Util. **40** (2020) 101223.
- [37] J.L. Venaruzzo, C. Volzone, M.L. Rueda, J. Ortiga, Microporous Mesoporous Mater. **56** (2002) 73.
- [38] C. Pevida, M.G. Plaza, B. Arias, J. Feroso, F. Rubiera, J.J. Pis, Appl. Surf. Sci. **254** (2008) 7165.
- [39] C. Chen, J. Kim, D.-A. Yang, W.-S. Ahn, Chem. Eng. J. **168** (2011) 1134.
- (Rec. 22/12/2020, Rev. 14/02/2021, 18/04/2021, Ac. 04/06/2021)